Available online at www.sciencedirect.com
ScienceDirect
Journal of Catalysis 246 (2007) 301–307
JOURNAL OF CATALYSIS
www.elsevier.com/locate/jcat

Ultrasound-assisted preparation of a highly active and selective Co-B amorphous alloy catalyst in uniform spherical nanoparticles

Hexing Li [a,*], Hui Li [a], Jing Zhang [a], Weilin Dai [b], Minghua Qiao [b]

[a] *Department of Chemistry, Shanghai Normal University, Shanghai 200234, PR China*
[b] *Department of Chemistry, Fudan University, Shanghai 200433, PR China*

Received 6 October 2006; revised 13 December 2006; accepted 17 December 2006

Available online 22 January 2007

Abstract

Uniform spherical Co-B amorphous alloy nanoparticles were prepared by ultrasound-assisted reduction of $Co(NH_3)_6^{2+}$ with BH_4^- in aqueous solution, and the particle size was adjusted by changing either the ultrasound power or the ultrasonication time. During liquid-phase cinnamaldehyde (CMA) hydrogenation, the as-prepared Co-B catalyst exhibited much higher activity and better selectivity to cinnamyl alcohol (CMO) than the regular Co-B obtained by direct reduction of Co^{2+} with BH_4^-. The higher activity can be attributed to both the higher dispersion of Co active sites (S_{Co}) and the higher intrinsic activity (R^S). The higher selectivity can be attributed to both the uniform Co-B amorphous alloy particles and the strong electronic interaction between Co and B, which enhances the competitive adsorption of C=O group against C=C group in the CMA molecule. Meanwhile, the stronger adsorption for hydrogen on Co active sites was more favorable for C=O hydrogenation in comparison with the C=C hydrogenation.

Keywords: Sonochemical preparation; Co-B amorphous alloy catalyst; Uniform particles; Cinnamaldehyde; Hydrogenation; Cinnamyl alcohol

1. Introduction

Amorphous alloy catalysts have received much attention owing to their higher activity, better selectivity, and stronger sulfur resistance in many hydrogenation reactions. Co-B is one of the most widely studied of these catalysts [1–3]. Chemical reduction is most frequently used in preparing Co-B amorphous alloys [4–7]; however, the regular Co-B samples obtained via direct reduction of Co^{2+} by BH_4^- in aqueous solution usually display low surface area, broadly distributed particle size, and poor thermal stability against crystallization due to aggregation, because the reduction reaction is vigorous and exothermic [8,9]. At very low temperatures or in ethanol solution, the reaction between Co^{2+} and BH_4^- can proceed smoothly, providing the Co-B amorphous alloy catalysts with high surface area [10,11]. But very high amounts of boron oxides coexisting with the Co-B amorphous alloy are harmful to catalytic performance due to the coverage of the Co active sites. One promising approach to designing uniform Co-B amorphous alloy particles is to reduce cobalt complexes by BH_4^-, as is often used in preparing Ni-P amorphous alloys [12]. However, the poor reduction degree seems problematic. Ultrasonication has proven a useful technique for inducing chemical reaction and inhibiting particle agglomeration due to the chemical effects from acoustic cavitation, which produces unusual chemical environments [13–16].

In this paper, we report a Co-B amorphous alloy catalyst in uniform nanoparticles with controllable size prepared by ultrasound-assisted reduction of $Co(NH_3)_6^{2+}$ with BH_4^-. Such Co-B catalyst exhibits higher activity and even better selectivity than the regular Co-B obtained via traditional methods during liquid-phase cinnamaldehyde (CMA) hydrogenation to cinnamyl alcohol (CMO). This is of industrial importance because CMO is widely used in organic synthesis and in the production of perfumes, flavorings, pharmaceuticals, and other fine chemicals [17–22]. Correlation of the catalytic performance to the structural properties is discussed briefly based on various characterizations.

* Corresponding author. Fax: +86 21 64322272.
E-mail address: hexing-li@shnu.edu.cn (H. Li).

0021-9517/$ – see front matter
doi:10.1016/j.jcat.2006.12.014

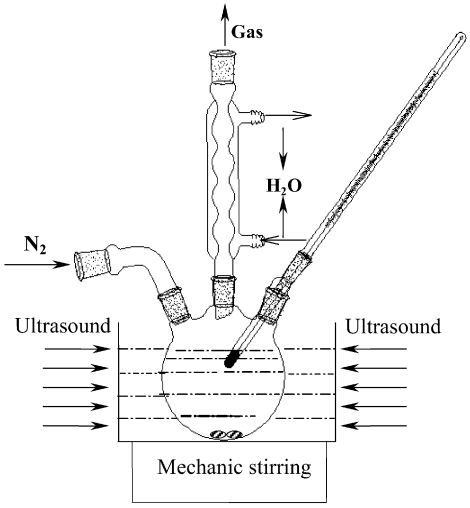

Fig. 1. A self-designed reactor used for sonochemical preparation of the Co-B catalyst.

2. Experimental

2.1. Catalyst preparation

Fig. 1 schematically illustrates the self-designed reactor used for sonochemical preparation of the Co-B sample. In the typical synthesis, 80 ml of 25% $NH_3{\cdot}H_2O$ solution was mixed with 20 ml of $CoCl_2$ solution containing 1.0 g of Co to form a $Co(NH_3)_6^{2+}$ complex. Then 32 ml of 2.0 M KBH_4 aqueous solution was added at 283 K in N_2 atmosphere. No significant reaction occurred in the absence of ultrasound-irradiation. Ultrasonication induced a smooth reduction of $Co(NH_3)_6^{2+}$ by BH_4^-, resulting in a black solid that was then washed thoroughly with H_2O and absolute alcohol (EtOH) and finally stored in EtOH until the time of use. The as-prepared Co-B samples were designated Co-B-x-y, where x and y represent ultrasound power (50, 75, and 100 W) and ultrasonication time (30 and 90 min), respectively. Ultrasound power <50 W or ultrasonication time <30 min was not used due to the incomplete reduction of the $Co(NH_3)_6^{2+}$ in aqueous solution. For comparison, the regular Co-B sample was also prepared via direct reduction of $CoCl_2$ by KBH_4 [5] and was designated Co-B-0.

2.2. Characterization

The bulk composition was analyzed by inductively coupled plasma optical emission spectrometry (ICP; Varian VISTA-MPX). The amorphous structure was determined by X-ray powder diffraction (XRD; Rigaku D/Max-RB with Cu$K\alpha$ radiation), selective area electronic diffraction (SAED; JEM-2010), and extended X-ray absorption fine structure (EXAFS; BL-10B). Surface morphology and particle size were evaluated by transmission electron microscopy (TEM; JEOL JEM2010). H_2 temperature-programmed desorption (TPD) and H_2 chemisorption were conducted on a Quantachrome CHEMBET-3000 system, from which the metallic surface area (S_{Co}) was calculated. The surface electronic states were investigated by X-ray photoelectron spectroscopy (XPS; Perkin–Elmer PHI 5000C ESCA using Al$K\alpha$ radiation), during which all of the Co-B samples were dried and pretreated in situ in pure Ar atmosphere to avoid oxidation. All of the binding energy values were calibrated using C 1s = 284.6 eV as a reference.

2.3. Activity test

Liquid-phase hydrogenation of CMA was carried out in a 500-ml stainless autoclave containing 5.0 g of catalyst, 15 ml of CMA, 105 ml of EtOH, and 1.0 MPa of H_2 at 383 K. The reaction system was stirred vigorously (1000 rpm) to eliminate the diffusion effect [25]. According to the P_{H_2} drop with the reaction time, both the specific activity (i.e., H_2 uptake rate per gram of cobalt; R^m = mmol/h g Co) and the areal activity (i.e., H_2 uptake rate per m^2 of the active surface area; R^S = mmol/h m^2 Co) were calculated by using the ideal gas equation. The R^S could be considered the intrinsic activity, because the effect of metal dispersion was excluded. During the reaction, the H_2 was refilled to maintain 1.0 MPa, and samples were withdrawn from the reaction mixture every 30 min for product analysis on a gas chromatograph (GC 102) with a flame ionization detector (FID) by means of 15% Apiezon (L)/Gas Chrom (red) at 523 K with N_2 as carrier gas, from which both the CMA conversion and the CMO yield could be determined. The reproducibility of the results was checked by repeating the runs at least three times and was found to be within acceptable limits (±5%).

3. Results and discussion

3.1. Structural and electronic characteristics

As shown in Fig. 2, the SAED pictures revealed that, similar to the regular Co-B (Co-B-0), the fresh Co-B samples prepared by the present method also displayed diffractional cycles indicative of the amorphous structure [26]. Meanwhile, the XRD patterns (Fig. 3) also demonstrated that both the fresh Co-B-50-30 and the fresh Co-B-0 samples were present in typical amorphous alloy structure, because only one broad peak around $2\theta = 45°$ was observed [27], which could be further confirmed by subsequent XPS and EXAFS characterizations. Treatment of the Co-B-50-30 at 773 K in N_2 flow for 2 h resulted in various diffractional peaks corresponding to both the metallic Co and the Co_2B alloy, implying crystallization, together with partial decomposition of the Co-B amorphous alloy. Further evidence for this conclusion was obtained from EXAFS.

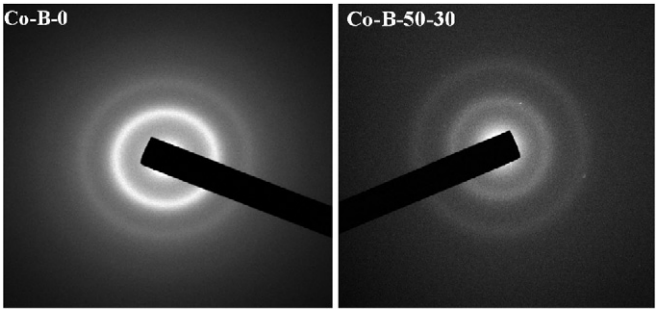

Fig. 2. SAED pictures of the fresh Co-B-0 and Co-B-50-30 samples.

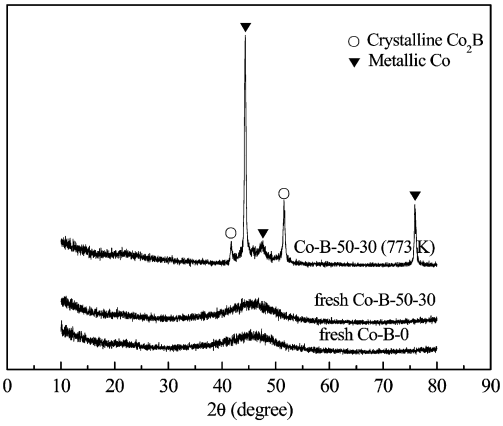

Fig. 3. XRD patterns of (a) the fresh Co-B-0, (b) the fresh Co-B-50-30, and (c) the Co-B-50-30 after being treated at 773 K in N_2 flow for 2 h.

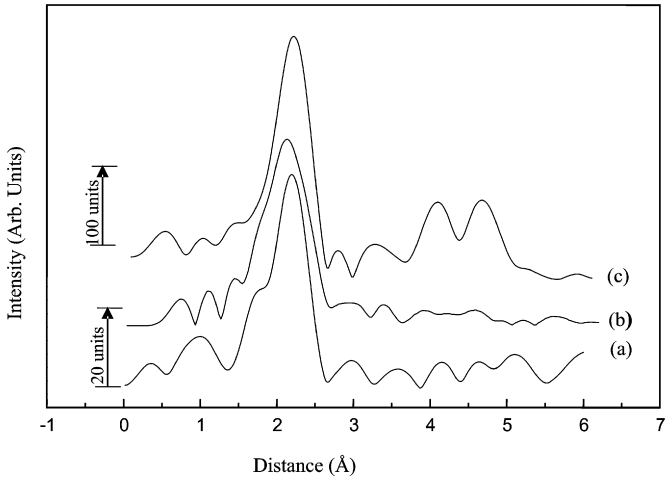

Fig. 4. RDF curves of (a) the fresh Co-B-0, (b) the fresh Co-B-50-30, and (c) the Co-B-50-30 after being treated at 773 K in N_2 flow for 2 h.

As shown in Fig. 4, the radial distribution functions (RDFs) obtained from the $Co\chi(k)k^3$ edge by fast Fourier transformation exhibited only one broad peak at around $R = 1.5$–2.5 Å for both the fresh Co-B-50-30 and fresh Co-B-0 samples, indicating that there was no long-range ordering structure but only the short-range ordering structure confined within the first-near-neighbor atom layer [28]. Meanwhile, a shoulder peak around 1.7 Å also demonstrated Co-B alloy formation [29]. Furthermore, calculations based on EXAFS revealed a much shorter Co-B bond length than the sum of the Co radius and the B radius, obviously due to formation of the Co-B alloy. After being treated at 773 K in N_2 flow for 2 h, the intensity of the original peak increased greatly, and two small additional peaks appeared at longer distances, indicating the transformation from the amorphous structure to the crystalline structure.

The TEM image (Fig. 5) revealed that the Co-B-0 sample was present in almost shapeless particles with extremely broad size distribution, from <10 nm to >300 nm. The presence of the large particles could be attributed to particle agglomeration [6], whereas the small particles could be attributed to the formation of boron oxides (as confirmed by the subsequent XPS spectra), which hampered the growing of Co particles. Unlike

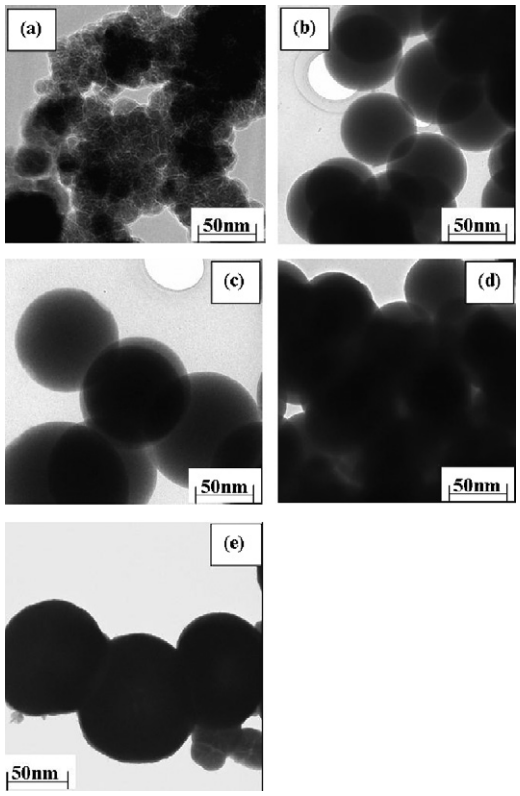

Fig. 5. TEM morphologies of the fresh Co-B samples. (a) Co-B-0, (b) Co-B-50-30, (c) Co-B-75-30, (d) Co-B-100-30, and (e) Co-B-50-90.

Co-B-0, Co-B-50-30 was present in uniform spherical nanoparticles of relatively larger sizes. The role of the ultrasonication can be interpreted in term of several factors. First, the intense shock waves resulting from the cavitation effect [30] could induce the reaction between $Co(NH_3)_6^{2+}$ complex and BH_4^- to produce the Co-B amorphous alloy. The agglomeration of Co-B particles could be avoided, because of the smooth reaction and the rapid movement of Co-B particles caused by these shock waves. Meanwhile, the formation, growth, and implosive collapse of bubbles in liquid induced by ultrasonication might create an extremely high energy level of localized supersaturation due to evaporation of the solvent in the bubbles at high temperature, which triggers nucleation [31]. Constant ultrasound power and irradiation time resulted in a similar microenvironment of localized supersaturation, possibly accounting for the uniform shape and particle size of the Co-B sample. As shown in Figs. 5c and 5d, the Co-B particle size increased with increasing ultrasound power due to the increased energy level of the localized supersaturation. Extremely extensive ultrasound power (100 W) or very long ultrasonication time (90 min) resulted in an abrupt increase in particle size and even the irregular particle shape (Figs. 5d and 5e), obviously due to the melting agglomeration during particle collisions [32].

The XPS spectra (Fig. 6) revealed that the cobalt species in all of the Co-B samples were present in the metallic state, whereas the boron species were present in two states, the B alloying with metallic $Co(B_{alloy})$ and the B oxide (B_2O_3). The boron oxide can be attributed to the hydrolysis of BH_4^- rather than the surface oxidation of the alloying B, because the prepa-

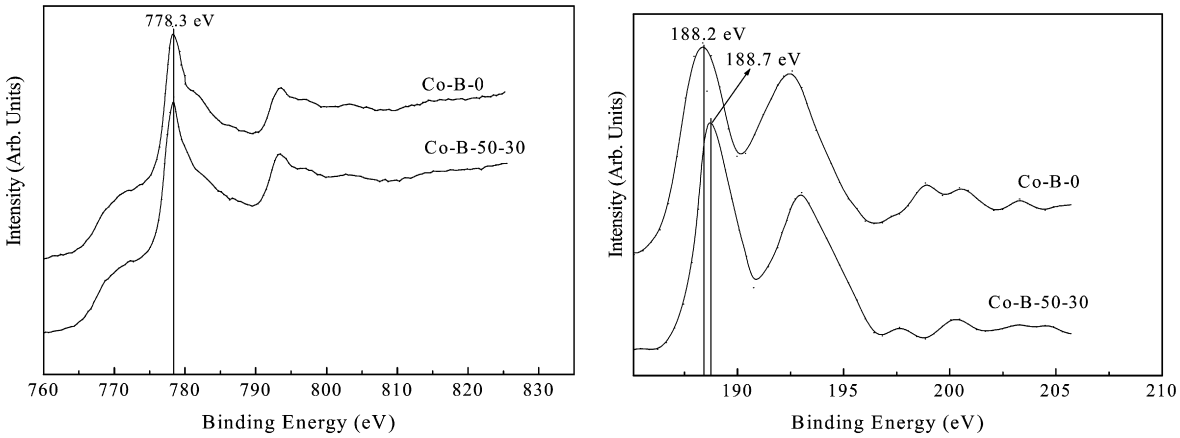

Fig. 6. XPS spectra of the fresh Co-B-0 and Co-B-50-30 samples.

Table 1
Structural and catalytic properties of different Co-B amorphous alloy catalysts[a]

Catalyst	Bulk comp. (atom%)	S_{Co} (m^2/g)	R^m (mmol/h g Co)	R^S (mmol/h m^2 Co)	Yield[b] (%)
Co-B-0	$Co_{75.4}B_{24.6}$	15.8	17.4	1.1	87.6
Co-B-50-30	$Co_{77.7}B_{22.3}$	25.5	40.8	1.6	91.2
Co-B-75-30	$Co_{78.3}B_{21.7}$	17.3	26.0	1.5	90.7
Co-B-100-30	$Co_{78.2}B_{21.8}$	8.1	13.0	1.6	89.0
Co-B-50-90	$Co_{77.9}B_{22.1}$	5.3	8.5	1.6	89.3
Crystallized Co-B-50-30[c]	$Co_{77.7}B_{22.3}$	9.4	7.7	0.82	76.9

[a] Reaction conditions: catalyst, 5.0 g; CMA, 15 ml; EtOH, 105 ml; T, 383 K; P_{H_2}, 1.0 MPa; stirring rate, 1000 rpm.

[b] The maximum yield obtained under the present reaction conditions.

[c] Obtained by treating the Co-B-50-30 amorphous alloy at 773 K in N_2 flow for 2 h.

ration and treatment of all of the Co-B samples were carried out in an absolutely anoxic reactor. Based on the areas of the XPS peaks indicative of the B_{alloy} and the B oxide, the surface molar ratios of the alloying B to the metallic Co(B_{alloy}/Co) and the alloying B to the total B(B_{alloy}/B_{total}, $B_{total} = B_{alloy} + B$ oxide) were determined using 0.13 and 2.50 as the PHI sensitivity factors to B 1s and Co $2p_{3/2}$, respectively [23,24]. The surface B_{alloy}/Co ratio in the Co-B-50-30 was determined to be 32.3/67.7, much higher than that in the Co-B-0 (28.0/72.0), indicating that the Co-B-50-30 was more surface-enriched with the boron species than the Co-B-0. Meanwhile, the surface B_{alloy}/B_{total} ratio was much higher in the Co-B-50-30 (68/100) compared with the Co-B-0 (51/100), indicating that the Co-B-50-30 contained less B oxides, possibly attributed to the inhibition of BH_4^- hydrolysis during the ultrasound-assisted reduction of $Co(NH_3)_6^{2+}$ and the removal of the oxidized B species by ultrasound due to its cleaning effect. Thus, the Co-B sample prepared through the present method contained fewer impurities.

Compared with the standard binding energy (BE) of the pure B (187.1 eV), a positive BE shift was seen in the alloying B in both Co-B-0 (188.2 eV) and Co-B-50-30 (188.7 eV), implying partial electron transference from alloying B to metallic Co [5,33]. The BE of the alloying B in Co-B-50-30 was even 0.5 eV higher than that in Co-B-0. Estimation on the Auger parameters demonstrated that both samples displayed the similar "final state" values [α = BE (Co $2p_{3/2}$) + KE Co LMM] but quite different "initial state" values (β = KE Co LMM + BE Co $2p_{3/2}$ + 2BE Co 3s). Thus, the "final state" effect indicating dispersion degree might be insignificant. The BE shift at boron can be attributed mainly to the "initial state" effect resulting from the stronger electronic interaction between the metallic Co and the alloying B, making the B more electron-deficient and the Co more electron-enriched. The failure to observe the BE shift of the metallic Co can be understood by considering its relatively greater atomic weight compared with the B atom [23].

The hydrogen TPD curves (Fig. 7) for Co-B-50-30 exhibit only one hydrogen desorption peak at around 600 K, implying that it contains unique Co active sites. In contrast, Co-B-0 displays four hydrogen desorption peaks at around 493, 593, 640, and 822 K. Thus, we can conclude that the Co-B-0 sample might contain at least four kinds of Co active sites, possibly corresponding to the metallic Co and the Co_2B, Co_3B, and Co_4B_2 alloys [29].

Other structural parameters are summarized in Table 1. ICP analysis revealed that all of the Co-B samples prepared by ultrasound-assisted reduction of $Co(NH_3)_6^{2+}$ by BH_4^- exhibited similar bulk compositions regardless of the ultrasound power and the ultrasonication time. Co-B-50-30 exhibited higher Co content in the composition than Co-B-0, possibly due to a lower amount of B oxides. Co-B-50-30 had a significantly greater metallic area (S_{Co}) than Co-B-0, obviously due to good dispersion of the Co-B particles. Further increases in ultrasound power resulted in decreased S_{Co} due to the increasing Co-B particle size. Extremely extensive ultrasound power (100 W)

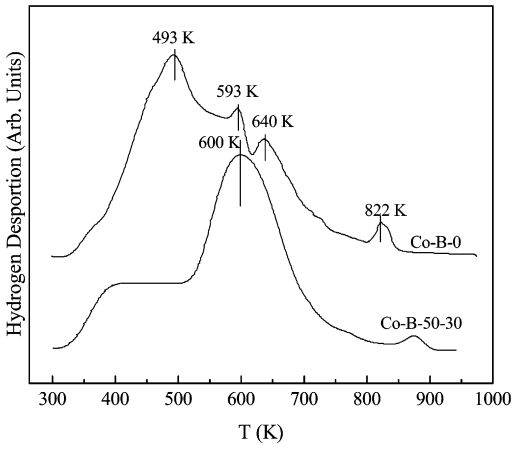

Fig. 7. Hydrogen TPD curves of the fresh Co-B-0 and Co-B-50-30 samples.

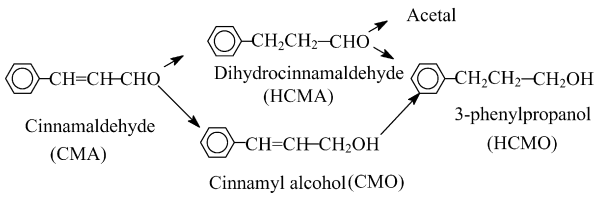

Scheme 1. A plausible reaction mechanism of the CMA hydrogenation.

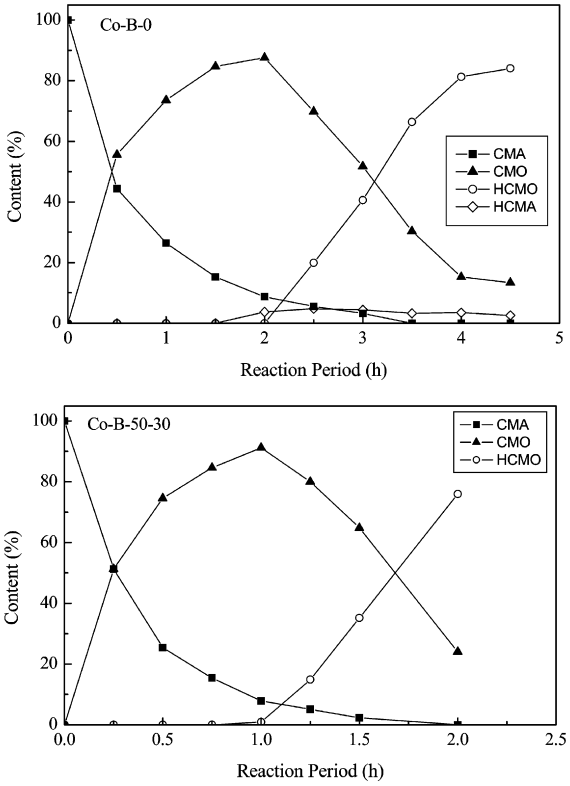

Fig. 8. Reaction profiles of the CMA hydrogenation over the Co-B-0 and the Co-B-50-30 amorphous alloy catalysts. Reaction conditions: catalyst, 5.0 g; CMA, 15 ml; EtOH, 105 ml; T, 383 K; P_{H_2}, 1.0 MPa; stirring rate, 1000 rpm.

or very long ultrasonication time caused an abrupt drop in S_{Co}, obviously due to the melting agglomeration of the Co-B alloy particles, as shown in Fig. 5.

3.2. Catalytic performance

CMA hydrogenation has been widely studied; a plausible reaction route is described in Scheme 1 [34,35]. Besides the main product CMO, the competitive hydrogenation of the C=C against the C=O in the CMA molecule resulted in dihydrocinnamaldehyde (HCMA) byproduct, and the further hydrogenation of either the CMO or the HCMA resulted in another byproduct, 3-phenylpropanol (HCMO). The CMA hydrogenation curves over the Co-B-0 and Co-B-50-30 amorphous alloy catalysts given in Fig. 8 clearly show that Co-B-50-30 exhibits much higher activity and better selectivity to CMO than Co-B-0. Other catalytic properties are summarized in Table 1. The maximum CMO selectivity (99.0% at CMA conversion of 92.1%) was obtained on Co-B-50-30. This value is much higher than those values obtained on the Raney Co catalyst (70.0 and 23.0% at CMA conversions of 70.8 and 98.7%, respectively) [36] under similar reaction conditions. The superior catalytic properties of the as-prepared catalysts compared with the Raney Co catalyst can be attributed to their favorable amorphous structure, supported by the fact that fresh Co-B-50-30 exhibited much higher R^m and R^S, as well as selectivity to CMO, than the corresponding crystallized catalyst obtained by treating the fresh catalyst at 773 K in N_2 flow for 2 h.

The greater activity of Co-B-50-30 compared with Co-B-0 can be attributed to the enhanced dispersion of the Co active sites (see the S_{Co} values) and intrinsic activity (see the R^S values). Increases in ultrasound power or ultrasonication time had no significant influence on R^S, but did result in a decrease in overall hydrogenation activity (R^m) due to the decreased S_{Co}.

The higher selectivity to CMO on Co-B-50-30 than on Co-B-0 can be attributed mainly to the absence of HCMA byproduct resulting from hydrogenation of the C=C group in the CMA molecule. These results can be explained by considering the following factors.

1. The TEM morphologies (Fig. 5) demonstrated the presence of Co-B-50-30 in uniform spherical particles of relatively larger size, which could inhibit the adsorption of the C=C due to steric hindrance from the neighboring benzene ring [34] and, in turn, inhibit the hydrogenation of C=C, resulting in increased selectivity to CMO.
2. According to the hydrogen TPD curves (Fig. 7), Co-B-50-30 contained only one kind of Co active site. Meanwhile, comparing the positions of the principal hydrogen desorption peaks clearly shows stronger hydrogen adsorption for Co-B-50-30 than for Co-B-0. The hydrogen atoms strongly adsorbed on the Co active sites were favorable for the competitive hydrogenation of the C=O group against the C=C group [37] coexisting in the CMA molecule, resulting in the higher selectivity to CMO. This also can account for the higher R^S of Co-B-50-30 compared with Co-B-0.
3. Blyholder and Shibabi confirmed that a metal–oxygen bond rather than a metal–carbon bond was responsible for the bonding between the carbonyl group and Co metal [38]. Meanwhile, Noller and Lin also confirmed that the C=O

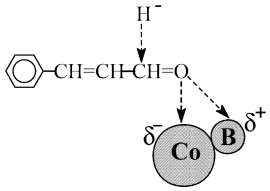

Scheme 2. A plausible model of CMA adsorption and hydrogenation on the Co-B.

hydrogenation started from the attack of H^- on the C atom [39]. Thus, the adsorption of the C=O group and its hydrogenation over the Co-B amorphous alloy catalyst can be described in the model shown in Scheme 2 [25].

The XPS spectra (Fig. 6) show that Co-B-50-30 exhibited a stronger electronic interaction between the metallic Co and the alloying B compared with Co-B-0, making the Co more electron-enriched and the alloying B more electron-deficient. On one hand, adsorption of hydrogen on the Co active sites with higher electron density might facilitate the formation of H^- species [39] and thus, enhance hydrogenation activity toward the C=O group. On the other hand, the electronic interaction between the C=O group and the Co active sites was the forward donation from the highest occupied molecular orbital (HOMO) of the C=O bonding (i.e., from 5σ of the O atom to the surface d_z2 and s orbitals of the Co atom) and the back-donation from the $d_x2_{-y}2$ orbital of the Co atom to the LUMO (i.e., $\pi^*_{C=O}$) [40]. Because $\pi^*_{C=O}$ is an antibonding orbital, the increased back-donation due to the higher electron density on the Co atom could weaken the C=O bond, favoring the dissociation of the C=O bond. In addition, the more electron-deficient B alloying with the metallic Co could further enhance the adsorption for the C=O group via a side-bond interaction (Scheme 2), thereby activating the C=O bond. Meanwhile, ultrasound treatment increased the dispersion and thus increased hydrogen and/or C=O adsorption as well as the back-donation of electrons to the antibonding orbital, because electron transfer is facilitated on the kink, corner sites. These results also can account for the higher intrinsic activity (R^S) and better selectivity to CMO on Co-B-50-30 compared with Co-B-0.

4. Conclusion

The ultrasound-assisted chemical reduction of $Co(NH_3)_6^{2+}$ by BH_4^- in aqueous solution has proven to be a promising approach to designing uniform spherical Co-B amorphous alloy particles of controllable size. Such a Co-B catalyst exhibited much higher activity and better selectivity to CMO during liquid-phase CMA hydrogenation compared with regular Co-B prepared by direct reduction of Co^{2+} with BH_4^-. This finding can be attributed to (1) the single type of Co active site; (2) the uniform Co-B alloy particles with relatively large size, which might inhibit adsorption for the C=C group in the CMA molecule and thus inhibit C=C hydrogenation to form HCMA; (3) the strong electronic interaction between the metallic Co and the alloying B, resulting in more electron-enriched Co and more electron-deficient B, which enhance the adsorption and activation of both hydrogen and the C=O group in the CMA molecule; and (4) the strong adsorption of the hydrogen, which is favorable for competitive hydrogenation of the C=O against the C=C coexisting in the CMA molecule. The optimum ultrasound power and ultrasonication time were determined to be 50 W and 30 min (i.e., Co-B-50-30). Extremely extensive ultrasound power or very long ultrasonication time is harmful for both the activity and selectivity to CMO due to melting agglomeration of the Co-B particles.

Acknowledgments

This work was supported by the National Natural Science Foundation of China (20377031, 20603023), the Preliminary 973 Project (2005CCA01100), the Shanghai Science and Technology Committee (05QMX1442, 0552nm036), and the Shanghai Eduction Committee (T0402, 05DZ20).

References

[1] A. Molnar, G.V. Smith, M. Bartok, Adv. Catal. 36 (1989) 329.
[2] Y. Chen, Catal. Today 44 (1998) 3.
[3] J.F. Deng, H.X. Li, W.J. Wang, Catal. Today 51 (1999) 113.
[4] A.H. Uken, C.H. Bartholomew, J. Catal. 65 (1980) 402.
[5] H.X. Li, Y. Wu, H. Luo, M. Wang, Y. Xu, J. Catal. 214 (2003) 15.
[6] H.X. Li, H. Li, W.L. Dai, M.H. Qiao, Appl. Catal. A Gen. 238 (2003) 119.
[7] H.X. Li, H. Li, M. Wang, Appl. Catal. A Gen. 207 (2001) 129.
[8] J.Y. Shen, Z.Y. Li, Q.J. Yan, Y. Chen, J. Phys. Chem. 97 (1993) 8504.
[9] H.X. Li, H. Luo, W.L. Dai, M.H. Qiao, J. Mol. Catal. A Chem. 203 (2003) 267.
[10] Y.Z. Chen, J.S. Wu, J. Chin. Inst. Chem. Eng. 23 (1992) 119.
[11] Z.B. Yu, M.H. Qiao, H.X. Li, J.F. Deng, Appl. Catal. A Gen. 163 (1997) 1.
[12] H.X. Li, W.J. Wang, H. Li, J.F. Deng, J. Catal. 194 (2000) 211.
[13] K.S. Suslick, S.B. Choe, A. Cichowlas, M.W. Grinstaff, Nature 353 (1991) 414.
[14] P. Mulvaney, M. Cooper, F. Grieser, D. Meisel, J. Phys. Chem. 94 (1990) 8339.
[15] N.A. Dhas, A. Gedanken, Chem. Mater. 9 (1997) 3144.
[16] L.H. Thompson, L.K. Doraiswamy, Ind. Eng. Chem. Res. 38 (1999) 1215.
[17] T.B.L.M. Marinelli, S. Nabuurs, V. Ponec, J. Catal. 151 (1995) 431.
[18] A. Ghosh, R. Kumar, Micropor. Mesopor. Mater. 87 (2005) 33.
[19] X.Q. Wang, R.Y. Saleh, U.S. Ozkan, J. Catal. 231 (2005) 20.
[20] Á. Zsigmond, I. Balatoni, K. Bogár, F. Notheisz, F. Joó, J. Catal. 227 (2004) 428.
[21] S.I. Fujita, Y. Sano, B.M. Bhanage, M. Arai, J. Catal. 225 (2004) 95.
[22] F. Delbecq, P. Sautet, J. Catal. 220 (2003) 115.
[23] H. Li, H.X. Li, W.L. Dai, Z. Fang, J.F. Deng, Appl. Surf. Sci. 152 (1999) 25.
[24] Physical Electronic Division, Perkin–Elmer, Operator's Reference Manual for PHI PC Windows Software Version 1.2b, p. 274.
[25] H.X. Li, X. Chen, Y. Xu, Appl. Catal. A Gen. 225 (2002) 117.
[26] S. Klein, J.A. Martens, R. Parton, K. Vercruysse, P.A. Jacobs, W.F. Maier, Catal. Lett. 38 (1996) 209.
[27] A. Yokoyama, H. Komiyama, H. Inoue, T. Masumoto, H.M. Kimura, J. Catal. 68 (1981) 355.
[28] J.A. Schwarz, C. Contescu, A. Contescu, Chem. Rev. 95 (1995) 477.
[29] B. Shen, S. Wei, K. Fan, J.F. Deng, Appl. Phys. A 65 (1997) 295.
[30] K.S. Suslick, S.J. Doctycz, Science 247 (1990) 1067.
[31] S. Devarakonda, J.M.B. Evans, A.S. Myerson, Cryst. Growth Des. 3 (2003) 741.
[32] T. Prozorov, R. Prozorov, K.S. Suslick, J. Am. Chem. Soc. 126 (2004) 13,890.
[33] Z.G. Fang, B.R. Shen, K.N. Fan, Chin. J. Chem. Phys. 15 (2002) 17.
[34] T.B.L.M. Marinelli, V. Ponec, J. Catal. 156 (1995) 51.

[35] Y. Nitta, Y. Hiramatsu, T. Imanaka, Chem. Express 4 (1989) 281.
[36] B.J. Liu, L.H. Lu, T.X. Cai, K. Iwatani, Appl. Catal. A 180 (1999) 105.
[37] H. Hu, M. Qiao, S. Wang, K. Fan, H.X. Li, B. Zong, X. Zhang, J. Catal. 221 (2004) 612.
[38] G. Blyholder, D. Shihabi, J. Catal. 46 (1977) 91.
[39] H. Noller, W.M. Lin, J. Catal. 85 (1984) 25.
[40] E. Boellaard, R.J. Vreeburg, O.L.J. Gijzeman, J.W. Geus, J. Mol. Catal. 92 (1994) 299.